

X-RAYING THE INTERGALACTIC O VI ABSORBERS

Y. YAO¹, T. M. TRIPP², Q. D. WANG², C. W. DANFORTH¹, C. R. CANIZARES³,
J. M. SHULL¹, H. L. MARSHALL³, AND L. SONG²

Accepted for publication in the *Astrophysical Journal*

ABSTRACT

The observed intergalactic O VI absorbers at $z > 0$ have been regarded as a significant reservoir of the “missing baryons”. However, to fully understand how these absorbers contribute to the baryon inventory, it is crucial to determine whether the systems are collisionally ionized or photoionized (or both). Using the identified intergalactic O VI absorbers as tracers, we search for the corresponding X-ray absorption lines, which are useful for finding the missing baryons and for revealing the nature of the O VI absorbers. Stacking the *Chandra* grating spectra along six AGN sight lines, we obtain three spectra with signal-to-noise ratios of 32, 28, and 10 per 12.5 mÅ spectral bin around the expected O VII K α wavelength. These spectra correspond to O VI absorbers with various dynamic properties. We find no detectable Ne IX, O VII, O VIII, N VII, or C VI absorption lines in the spectra, but the high counting statistics allows us to obtain firm upper limits on the corresponding ionic column densities (in particular $N_{\text{OVII}} \lesssim 10 N_{\text{OVI}}$ on average at the 95% confidence level). Jointly analyzing these non-detected X-ray lines with the averaged O VI column density, we further limit the average temperature of the O VI-bearing gas to be $T \lesssim 10^{5.7}$ K in collisional ionization equilibrium. We discuss the implications of these results for physical properties of the putative warm-hot intergalactic medium and its detection in future X-ray observations.

Subject headings: Cosmology: observations — intergalactic medium — quasar: absorption lines — X-rays: general

1. INTRODUCTION

Hydrodynamic simulations of cosmic large-scale structure indicate that, in the local universe ($z \lesssim 1$), the shock-heated gas in the tenuous warm-hot intergalactic medium (WHIM) at temperatures $T \sim 10^{5-7}$ K contains a substantial amount of baryonic matter (Cen & Ostriker 1999; Davé et al. 2001), providing a possible solution for the so-called “missing baryons” problem (e.g., Persic & Salucci 1992; Fukugita et al. 1998). In a collisionally ionized gas at these temperatures, the most abundant heavy elements (e.g., C, N, O, and Ne) are in their high ionization (e.g., Li-, He-, and H-like) states (Sutherland & Dopita 1993), whose K- and L-shell transitions are in the X-ray and far-ultraviolet (far-UV) wavelength bands, respectively. The existence of the WHIM has been suggested through detections of X-ray emission from high-density regions near galaxies, groups, and clusters (e.g., Wang et al. 1997, 2004; Finoguenov et al. 2003; Sołtan 2007; Mannucci et al. 2007; see also Durret et al. 2008 for a review), but these regions are expected to contain only a small portion of the WHIM gas. The majority is located in low-density cosmic-web filaments (Davé et al. 2001), whose emission is hard to detect with current X-ray and far-UV telescopes. These filaments are most easily probed through absorption lines imprinted on spectra of background sources.

With the high sensitivity spectrographs aboard the *Hubble Space Telescope* (HST) and the *Far Ultraviolet Spectroscopic Explorer* (FUSE), the intergalactic O VI absorption lines (at rest-frame wavelengths 1031.93 Å and 1037.62 Å) have routinely been detected in many background AGN spectra (e.g., Savage et al. 1998; Tripp et al. 2000; Tripp & Savage 2000; Shull et al. 2003; Prochaska et al. 2004; Danforth & Shull 2005; Cooksey et al. 2008). However, the nature of these O VI absorbers is still under debate. In a survey of the intergalactic medium (IGM) absorption lines, Danforth & Shull (2008) found a good correlation in column density and a similar power-law slope of the column density distribution dN/dz of O VI and N V, which are distinct from those of H I, C III, and Si III. These features, along with the theoretical expectations of high post-shock temperatures and long cooling times of the WHIM, motivated them to argue for a multiphase nature of the IGM. In this picture, O VI and N V trace the canonical WHIM at temperatures of 10^{5-6} K, while the low ionization ions like C II-C IV and Si II-Si IV are predominantly photoionized. But in two other independent surveys that include a number of common sight lines to those used by Danforth & Shull (2008), Tripp et al. (2008) and Thom & Chen (2008) found that 30-40% of the O VI absorbers have velocity centroids that are well aligned with those of the associated H I absorbers and that some absorber temperatures inferred from the line widths, $T < 10^5$ K, are well below that expected in the canonical WHIM. Tripp et al. (2008) also showed that these velocity-aligned absorbers can be naturally explained by photoionization models. These latter findings are consistent with previous investigations along individual sight lines based on the kinematic and chemical

¹Center for Astrophysics and Space Astronomy, University of Colorado, 389 UCB, Boulder, CO 80309; yangsen.yao, michael.shull, charles.danforth@colorado.edu

²Department of Astronomy, University of Massachusetts, Amherst, MA 01003; tripp, wqd, limin@astro.umass.edu

³Massachusetts Institute of Technology (MIT) Kavli Institute for Astrophysics and Space Research, 70 Vassar Street, Cambridge, MA 02139; crc, hermanm@space.mit.edu

properties of the high- and low-ionization absorbers (e.g., Tripp & Savage 2000; Savage et al. 2002; Sembach et al. 2004; Prochaska et al. 2004; Lehner et al. 2006). However, the UV data usually do not have high enough quality to uniquely constrain the ionization mechanism; Tripp et al. (2008) also showed that the O VI lines could alternatively arise in hot interface layers on the surface of low-ionization clouds if the O VI systems are always multiphase media. Current data cannot rule out this possibility, and many O VI absorbers are fully consistent with this hypothesis (see § 4.2 in Tripp et al. 2008). So far, the strongest indication of the collisional ionization origin of the O VI absorbers is the detection of Ne VIII absorption lines (at rest-frame wavelengths 770.4 Å and 780.3 Å) toward HE 0226-4110 at $z_a = 0.2070$ and toward 3C 263 at $z_a = 0.3257$ (Savage et al. 2005; Narayanan et al. 2008). However, a systematic search toward other sight lines has failed to find similar systems (Lehner et al. 2006).

The claimed detections of the WHIM in the X-ray band are still controversial. In the spectrum of PKS 2155-304 observed with the *Chandra* Advanced CCD Imaging Spectrometer (ACIS), Fang et al. (2002) reported an O VIII K α absorption line at $z = 0.0553$, claiming the first detection of the WHIM in the X-ray. This detection has not been confirmed, although it cannot be ruled out either, by the *Chandra* High Resolution Camera (HRC) observations and the subsequent *XMM-Newton* Reflection Grating Spectrometer (RGS) observations (Cagnoni et al. 2004; Williams et al. 2007; Fang et al. 2007). Nicastro et al. (2005) reported detections of two $z > 0$ O VII WHIM systems in the *Chandra* spectra of Mrk 421, which were not confirmed from the *XMM-Newton* RGS observations of the same source (Kaastra et al. 2006; Rasmussen et al. 2007). Kaastra et al. (2006) also questioned the statistical significance of the Mrk 421 detections in the *Chandra* spectra. The other claimed $z > 0$ X-ray WHIM absorptions are mostly detected at marginal significance (e.g., Mathur et al. 2003). Very recently, Buote et al. (2009) have reported a 3σ detection of O VII K α absorption affiliated with a large-scale structure (the Sculptor Wall). The O VII and O VIII absorption lines at $z \simeq 0$, which may be partially due to the WHIM in the Local Group (e.g., Nicastro et al. 2002; Fang et al. 2003), have been relatively well detected, but these absorptions are severely confused by the contributions from the Galactic hot gas close to (or within) the Milky Way disk (Sembach et al. 2003; Yao & Wang 2005, 2007; Wang et al. 2005; Fang et al. 2006; Bregman & Lloyd-Davies 2007; Yao et al. 2008).

With the controversial X-ray detections of the WHIM and the debatable nature of the observed far-UV absorbers, two key questions still remain open: (1) Does the WHIM exist? (2) If it does, what are its physical properties?

The highly ionized X-ray absorption lines are believed to be useful for finding the WHIM gas and for probing the nature of the O VI absorbers. The O VII ion can trace gas over a broad temperature range, and its column density is expected to be $\gtrsim 10$ times higher than that of O VI in a shock-heated gas with shock temperatures $T \gtrsim 10^{5.7}$ K (for overdensity $\delta \sim 10 - 100$; e.g., Furlanetto et al. 2005). Moreover, cosmological simula-

tions predict that hot O VI absorbers should have comparably strong (or even stronger) affiliated O VII absorption lines (see, e.g., Figures 8-10 in Cen & Fang 2006 and Figure 14 in Chen et al. 2003). However, because of the limited sensitivity and spectral resolution of the current X-ray observatories like *Chandra* and *XMM-Newton*, searching for X-ray lines in the WHIM is currently a difficult task. For instance, the column densities of the X-ray absorbing ions, even for the most promising one (O VII), are expected to be small with $N_{\text{OVII}} \approx 10^{15} \text{ cm}^{-2}$ (e.g., Chen et al. 2003). For the most part, the background AGN are also relatively faint in the X-ray band. Consequently, very long exposures (see § 5) are required to collect enough photons to conduct a blind search for X-ray absorption lines from the WHIM along a random line of sight. These difficulties contribute to the controversies and frustrations surrounding the reported X-ray detections.

In this work, we search for the X-ray absorption lines of O VII, as well as O VIII, Ne IX, N VII, and C VI, by extensively exploring the archived *Chandra* grating observations. We use the identified O VI absorbers as tracers to avoid uncertainties of a blind search. We also develop a technique to stack all the applicable X-ray observations and obtain spectra with unprecedented counting statistics.

The paper is organized as follows. In § 2, we list the identified O VI absorbers and the corresponding *Chandra* observations utilized in this work, and describe the data reduction process. In § 3, we present our search method and stack the X-ray observations in the rest frame of the observed O VI absorbers. We search for the X-ray absorption lines in the stacked spectra, present the results of the data analysis in § 4, and discuss the implications of our results in § 5.

2. O VI ABSORBERS, CHANDRA OBSERVATIONS, AND DATA REDUCTION

There are ~ 80 identified IGM O VI systems at redshifts of $0 < z_{\text{abs}} < 0.5$ toward ~ 30 AGN sight lines (Savage et al. 2002; Sembach et al. 2004; Danforth et al. 2006; Danforth & Shull 2005, 2008; Tripp et al. 2008; Thom & Chen 2008). *Chandra* has observed 12 of these AGN with high spectral resolution grating instruments. To avoid the potential confusion caused by the absorbers intrinsic to the AGN in identifying the IGM O VI systems and in searching for X-ray lines, we do not use the five AGN (Mrk 279, NGC 5548, Mrk 509, Ark 564, and NGC 7469) toward which warm absorbers have been detected in the X-ray band (e.g., Scott et al. 2004, 2005; Kaastra et al. 2002; Yaqoob et al. 2003; Matsumoto et al. 2004). *Chandra* observations of the five AGN could contribute an additional $< 10\%$ in total to the spectral counts of our final spectra (see below), so excluding them in the data analysis does not significantly affect our results. To avoid the confusion caused by possible absorber misidentification or noise features, we only used the O VI systems that were detected at $> 3\sigma$ significance levels. We further excluded the *proximate* absorbers that are within $\sim 2,000 \text{ km s}^{-1}$ to the AGN redshifts; Tripp et al. (2008) have shown that the majority of the proximate O VI systems are found within this velocity interval at low redshifts. The proximate systems can be high-velocity AGN ejecta and/or can be located

near the central engine of the AGN. Consequently, these systems should be excluded when searching for WHIM absorbers.

Table 1 summarizes our O VI absorber sample, including the redshifts of the O VI systems (z_{OVI}), $\lambda 1031.93$ equivalent widths, dispersion velocities (b), and column densities (N_{OVI}) along the six sight lines used in this work. For those absorbers at very close redshifts along a single sight line that cannot be distinguished with the *Chandra* resolution, only the systems with higher EWs were used. Galaxy surveys at low z show that most of these O VI absorbers are usually found within several hundred kpc of intervening galaxies along the sight lines (Tripp & Savage 2000; Savage et al. 2002; Shull et al. 2003; Sembach et al. 2004; Tumlinson et al. 2005; Prochaska et al. 2006; Stocke et al. 2006; Tripp et al. 2006; Cooksey et al. 2008). The investigation of the connection between galaxy environment and X-ray absorbers is underway and will be presented in a separate paper. In this work, we focus on searching for corresponding X-ray absorption of the O VI-bearing gas.

We follow the criteria used in Tripp et al. (2008) to classify the O VI absorbers along the six AGN sight lines into *simple* and *complex* systems. In simple systems, the velocity centroids of H I and O VI are well aligned (within 2σ of their velocity uncertainties). In complex absorbers, these velocity centroids are well separated ($> 2\sigma$ apart) and/or there are multiple low- and high-ionization stages (e.g., C II-C IV, Si II-Si III, or N V, in addition to O VI) that indicate the presence of multiple ionization phases. We also classify the O VI absorbers with equivalent width (EW) > 80 mÅ as *strong* systems (e.g., Fang & Bryan 2001). Tripp et al. (2008) classified the O VI absorbers along three of the six sight lines. Using these criteria, we classified all the O VI absorbers reported by Danforth et al. (2006) and Danforth & Shull (2008) toward the other three sight lines. Figure 1 presents examples of each classified system.

As of 2008 May 6, there were ~ 100 archived *Chandra* grating observations of the six selected targets. In this work, we did not use non-standard observations with uncertain calibrations. We also excluded several short observations (with an individual exposure $\lesssim 10$ ks) of PKS 2155-304 that contribute $< 5\%$ to the total spectral counts of the source. Table 2 summarizes the number of observations and the total exposure used in this work.

For ACIS grating observations, we followed the procedures described in Yao & Wang (2005, 2007) to calibrate the data, extract spectra, and calculate corresponding response functions (RSPs). The same energy grid was applied throughout these procedures. We utilized the medium energy grating (MEG) spectra of the High Energy Transmission Grating (HETG; Canizares et al. 2005) observations and only used the first grating order spectra of all observations.

For each HRC grating observation, we followed the steps presented in Wang et al. (2005) to obtain the first order RSP (FRSP) and order-overlapped RSP (ORSP) and spectra. We then extracted the first order spectra by subtracting the difference of the best-fit-model predicted channel counts between the ORSP and the FRSP from the order-overlapped spectra.

Spectra from positive and negative grating arms of each observation were then co-added, and multiple observations toward a single sight line were further stacked to enhance the counting statistics. Visual inspection revealed no significant and consistent $K\alpha$ lines of O VII, O VIII, Ne IX, N VII, or C VI at the corresponding redshift z_{OVI} along individual sight lines. Figure 2 shows parts of the final spectra of the six AGN around the expected IGM O VII $K\alpha$ lines.

Spectra along the PKS 2155–304 sight line deserve to be mentioned particularly because of their excellent spectral quality (Fig. 2). Toward this sight line, Shull et al. (2003) detected two O VI absorption systems at redshifts $z = 0.054$ and 0.057 , associated with a cluster of seven H I absorbers and a group of galaxies (Shull et al. 1998). Figure 3 shows the detected O VI and other non-detected metal absorption lines along with the cluster of H I lines. On the *Chandra* ACIS-grating spectrum, the claimed $z = 0.0553$ O VIII line at $\lambda_{\text{obs}} = 20.02$ Å is clearly visible with an EW of $5.9(3.1, 8.6)$ mÅ (90% confidence range), which is consistent with that reported by Fang et al. (2002, 2007). There is no other X-ray line at this redshift. The discrepancy between the HRC-grating, the *XMM-Newton* RGS (with an accumulated exposure time of 980 ks), and the ACIS-grating spectra still exists; the former two spectra yield upper limits of $EW < 3.2$ mÅ and < 3.7 mÅ, respectively (see also § 1 and references therein). The line in the co-added HRC+ACIS spectrum is severely diluted with $EW < 4.2$ mÅ.

3. AN EFFECTIVE STACKING AND SEARCHING STRATEGY

To facilitate an effective search for X-ray IGM absorption lines, we first blueshifted the X-ray spectral data by the observed O VI absorber redshifts z_{OVI} and reconstructed the corresponding RSPs accordingly. The data are originally in forms of detected counts distributed in a wavelength grid that was chosen to be the same for all the X-ray spectra. The rest-frame wavelength λ_0 is related to the observed wavelength λ_{obs} by

$$\lambda_0 = \lambda_{\text{obs}} / (1 + z_{\text{OVI}}). \quad (1)$$

For each absorber, we first use this relationship to recalculate the grid boundaries of the corresponding X-ray spectrum and then cast the spectrum and the RSP onto a rest-frame spectral grid, which is chosen to be the original one. The re-calculated spectrum, both shifted and compressed, generally no longer matches this chosen rest-frame grid. Therefore, some of the re-calculated spectral bins fall completely within individual rest-frame grid intervals, whereas others enclose a grid boundary. In this latter case, we split the counts in such a bin into two parts and assign them to the two grid intervals adjacent to the enclosed boundary; the weights used in the splitting are proportional to the wavelength overlaps of the bin with the two intervals. In the same way, we re-calculate the wavelength boundaries and the distribution probability in the corresponding RSP file. We repeat this procedure for all the absorbers to obtain their respective rest-frame spectral and RSP files; for individual sight lines with n intervening O VI systems (Table 1), we obtained n shifted spectra and RSPs.

To enhance the counting statistics, we co-added these shifted spectra to form a single stacked spectrum and

TABLE 1
PROPERTIES OF THE IDENTIFIED O VI ABSORBERS

Source Name	z_{AGN}	z_{OVI}	EW (mÅ)	b (km s ⁻¹)	$\log[N_{\text{OVI}}(\text{cm}^{-2})]$	Class ^b
H1821+643	0.2970	0.0244	27 ± 8	21 ⁺⁹ ₋₆	13.44 ± 0.1	Sm
		0.1214	97 ± 14	76 ⁺¹³ ₋₁₁	13.97 ± 0.06	Cm, St
		0.2133	39 ± 9	28 ± 5	13.54 ± 0.06	Cm
		0.2250 ^a	190 ± 10	45 ± 2	14.27 ± 0.02	Cm, St
		0.2264 ^a	32 ± 4	16 ± 2	13.51 ± 0.04	Cm
		0.2453	51 ± 7	26 ± 2	13.71 ± 0.03	Sm
3C 273	0.1583	0.0033	31 ± 7	51 ⁺¹¹ ₋₉	13.44 ± 0.07	Cm
		0.0902	16 ± 3	22 ± 6	13.18 ± 0.06	Cm
		0.1200	24 ± 3	8 ± 3	13.37 ± 0.04	Sm
PG 1116+215	0.1765	0.0593	63 ± 9	36 ⁺¹¹ ₋₈	13.52 ± 0.08	Sm
		0.1385	83 ± 16	36 ± 7	13.97 ± 0.06	Cm, St
		0.1655	111 ± 9	32 ⁺²¹ ₋₁₃	14.08 ± 0.04	Cm, St
PKS 2155-304	0.1165	0.0540 ^a	32 ± 5	14 ± 6	13.63 ± 0.12	Cm
		0.0572 ^a	44 ± 11	24 ± 7	13.57 ± 0.09	Cm
Ton S180	0.0620	0.0456	62 ± 14	20	13.74 ± 0.06	Sm
PG 1211+143	0.0809	0.0511	187	53 ⁺¹⁰ ₋₉	14.21 ± 0.08	Cm, St
		0.0645 ^a	144 ± 32	54 ± 11	14.16 ± 0.08	Cm, St
		0.0649 ^a	55 ± 10	21	13.83 ± 0.11	Cm
averaged ^c			45.4	28	13.62	All
averaged ^d			49.0	32	13.65	Cm
averaged ^e			131.7	59	14.11	St

NOTE. — Errors are listed in 1σ range. The values of the first three sources (H1821+643, 3C 273, and PG1116+215) are adopted from Tripp et al. (2008), and the remaining values are adopted from Danforth & Shull (2008) except for those at the redshift 0.0511 along the PG 1211+143 sight line, which are adopted from Tumlinson et al. (2005). ^a Toward an individual sight line, these absorbers cannot be distinguished with *Chandra* resolution, and the system with higher equivalent width of O VI is used. ^b Classification of the O VI absorbers; “Cm”, “Sm”, and “St” denote complex, simple, and strong O VI systems, respectively. ^{c,d,e} Values are weight averaged with respect to the spectral counts at the O VII K α wavelength (21.602 Å) in the shifted spectra for all, complex, and strong O VI absorbers, respectively (§ 4).

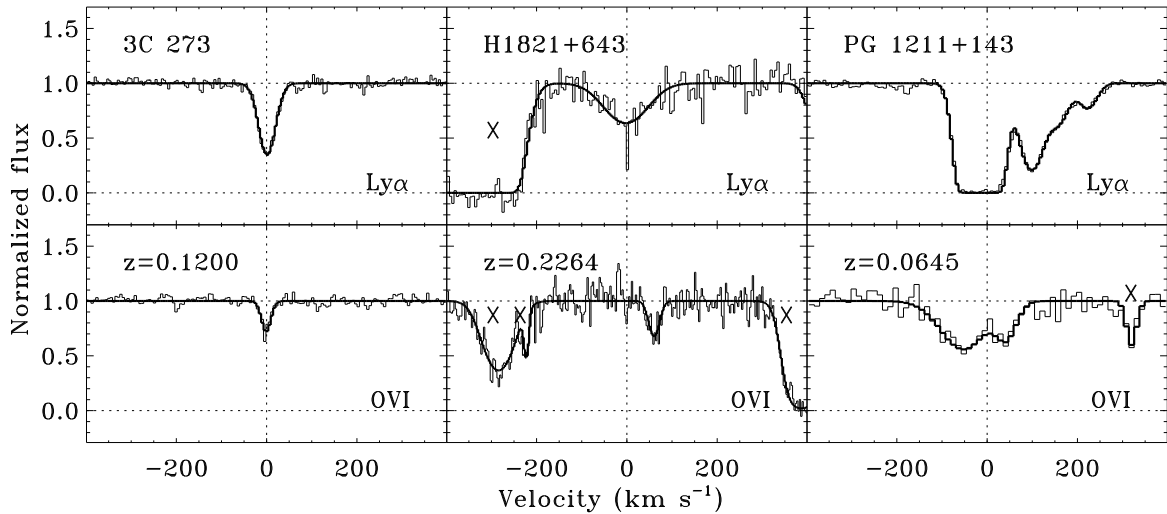


FIG. 1.— From left to right, examples of the simple, complex, and strong O VI absorbers and the corresponding Ly α systems, along the 3C 273, H1821+643, and PG 1211+143 sight lines (Tripp et al. 2008; Danforth & Shull 2008), respectively. Absorbers that are not associated with the labeled systems are marked with “X”.

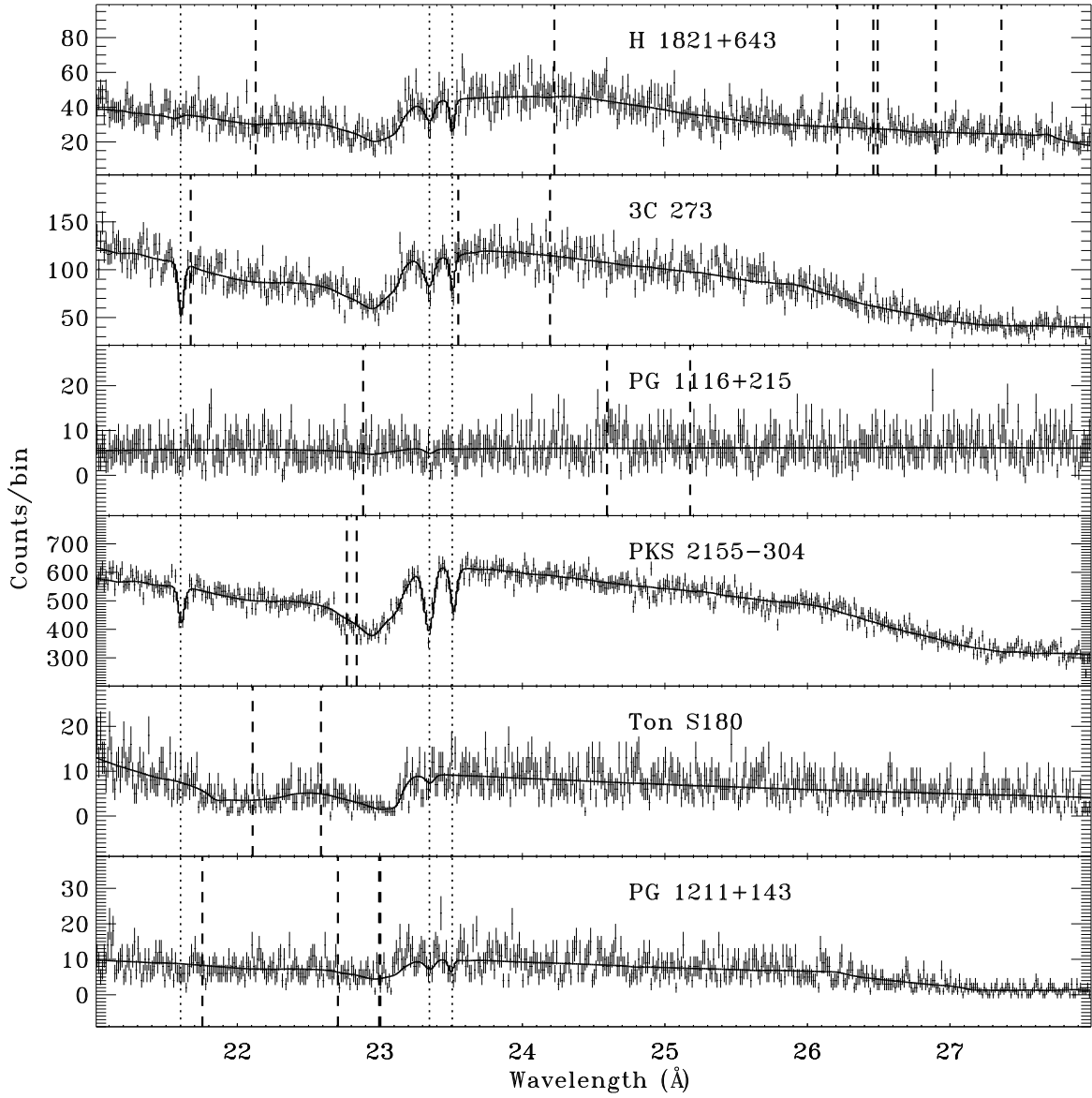


FIG. 2.— *Chandra* spectra of the six sources around the O VII $K\alpha$ line and the best-fit continua. The vertical dotted lines mark the Galactic O VII, O I, and O II $K\alpha$ lines at 21.602, 23.508, and 23.348 Å, respectively. The thick dashed lines mark the expected positions of the intergalactic O VII $K\alpha$ lines at the corresponding z_{OVI} (Table 1). The bin size is 12.5 mÅ.

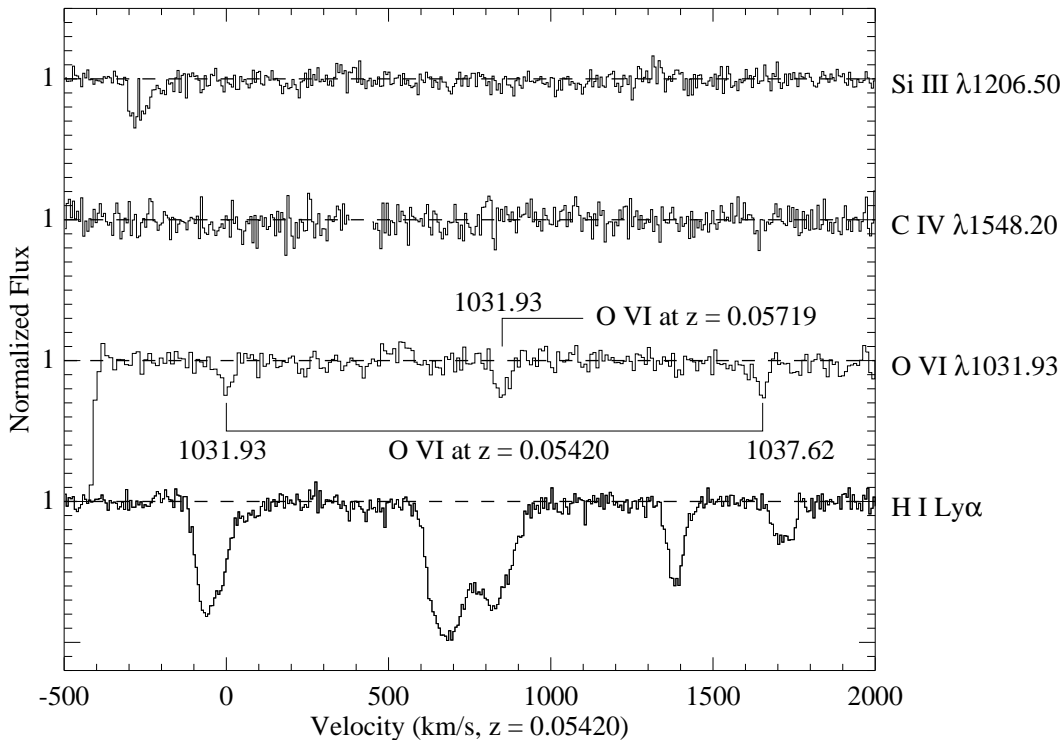


FIG. 3.— Metal absorption lines associated with a cluster of H I Ly α lines detected in the PKS 2155-304 spectrum, plotted vs. velocity with $v = 0 \text{ km s}^{-1}$ at $z_{\text{abs}} = 0.0542$. Both lines of the O VI doublet are clearly detected at $z_{\text{abs}} = 0.0542$ and are marked. Only the O VI $\lambda 1031.93$ transition is detected at $z_{\text{abs}} = 0.0572$, but the weaker O VI $\lambda 1037.62$ line is blended with a strong Galactic Fe II transition.

TABLE 2
Chandra GRATING OBSERVATIONS OF
THE SELECTED TARGETS

Src. Name	z_{AGN}	#. obs. (LETG)	Exp. (ks)
H1821+643	0.297	5	600
3C 273	0.158	16	360
PG 1116+215	0.176	1	89
PKS 2155-304	0.117	36	760
Ton S180	0.062	1	80
PG 1211+143	0.081	3	141
sub total:		62	2030

RSP. We constructed three different stacked spectra based on the various O VI absorber classifications (§2). Figure 4 illustrates the stacked spectrum that contains *all* of the shifted spectra corresponding to the 16 O VI systems used in this work (Table 1) regardless of their classification. Figure 5 presents the stacked spectrum for only the *complex* O VI systems, and Figure 6 is the stacked spectrum for only the strong O VI systems (Table 1). To avoid any potential bias in our results caused by the large contribution of the PKS 2155-304 sight line in the stacked spectra (Fig. 2) and by its peculiarity in detecting only the O VIII line (§ 1), we also obtained two similar stacked spectra and RSPs like those presented in Figures 4 and 5, but without the PKS 2155-304 contribution. For the same reasons, we also report two sets of results in the following sections when applicable, with and without the contribution of PKS 2155-304. It is interesting to point out that, because of the poor spectral

resolution of the X-ray instruments, absorbers at very close redshifts/velocities along a single sight line that cannot be distinguished with the *Chandra* LETG resolution ($\sim 750 \text{ km s}^{-1}$) are automatically stacked/merged as one velocity component.

Because each spectrum has been shifted by the corresponding z_{OVI} before being stacked, the X-ray IGM K α absorption lines of Ne IX, O VIII, O VII, N VII, and C VI, if they are associated with the O VI-bearing gas, are expected to be at rest-frame wavelengths of 13.448, 18.967, 21.602, 24.781, and 33.736 Å, respectively, in the stacked spectra.

4. ANALYSIS AND RESULTS

We now search for and measure the X-ray absorption lines in the stacked spectra. There are no extragalactic O VII, O VIII, Ne IX, N VII, or C VI absorption lines apparent in any of the stacked spectra (Figs. 4–6). Adding Gaussian profiles at the corresponding rest-frame wavelengths, we obtain upper limits to EWs of these lines. To obtain column densities of these ions, we first calculate the mean dispersion velocity (\bar{b}) and column density $\overline{N_{\text{OVI}}}$ of different classified O VI systems (Table 1) by weighting them with respect to the spectral counts at the wavelengths of the expected O VII K α lines (Fig. 2). Replacing the Gaussian profiles with the absorption line model *absline*⁴ (Yao & Wang 2005) and fixing the b of

⁴ In modeling a single absorption line, this model is similar to the curve-of-growth analysis. But it can be used to jointly analyze multiple absorption lines at the same time. For a detailed

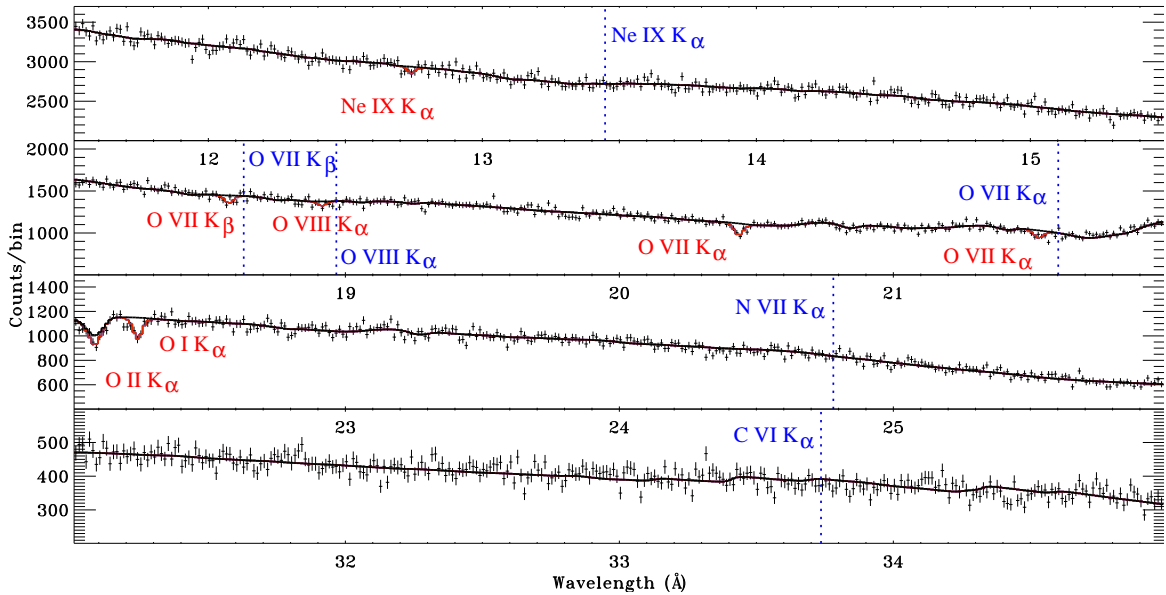


FIG. 4.— Four ranges of the final stacked spectrum that includes shifted spectra corresponding to all 16 O VI systems (Table 1). The thick lines mark the best-fit continuum, the red lines and text mark the blue-shifted Galactic absorptions (mainly contributed from PKS 2155–304 and 3C 273 sight lines), and blue vertical lines mark the positions of the expected intergalactic neon, oxygen, nitrogen, and carbon absorption lines at the corresponding rest-frame wavelengths. The bin-size is 12.5 mÅ.

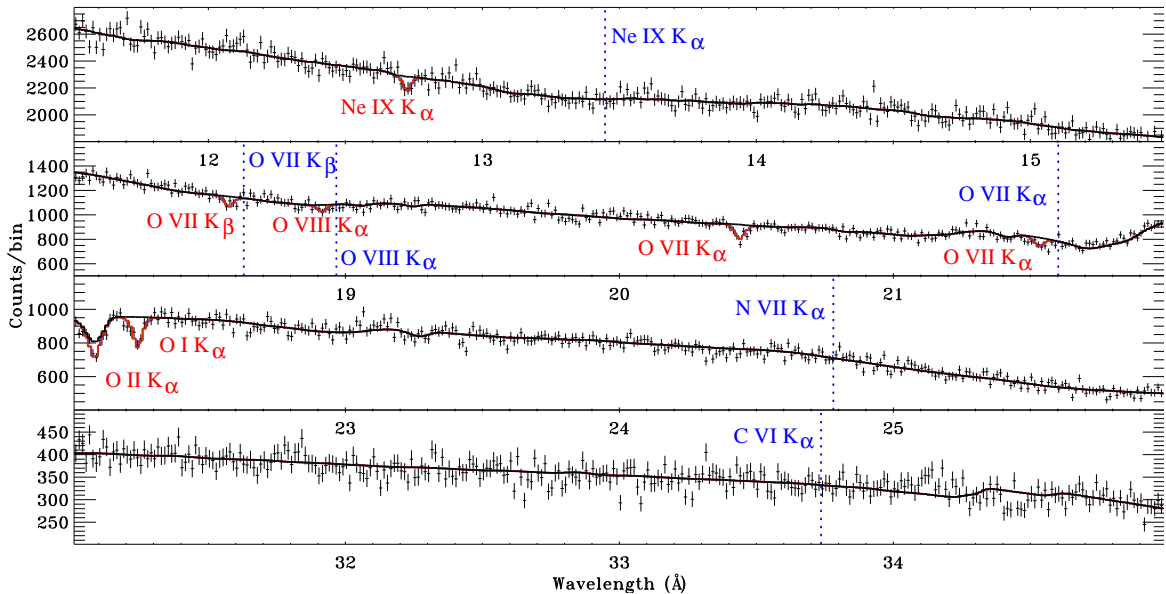


FIG. 5.— Same as Figure 4, except that stacked spectrum contains only spectra corresponding to the complex O VI systems (Table 1).

different ions to \bar{b} , we then estimate the column density upper limits of these ions as reported in Table 3.

With these upper limits to the ionic column densities and calculated \bar{N}_{OVI} , we can probe thermal properties of the O VI-bearing gas. For a gas in collisional ionization equilibrium (CIE), the column density ratio between O VII and O VI provides a diagnostic of gas temperature (Sutherland & Dopita 1993; Yao & Wang 2005). Assuming a single gas temperature, we jointly analyze the non-detected O VII with the \bar{N}_{OVI} (Tables 1 and 3), and obtain a temperature upper limit of $\log[T(\text{K})] < 5.7$ at the 95% confidence level from the three spectra corre-

description of the model, see Yao & Wang (2005).

sponding to all, complex, and strong O VI absorbers. Including the non-detected lines of Ne IX, N VII, and C VI in the joint analysis (assuming relative solar abundances of Ne/O, N/O and C/O; Anders & Grevesse 1989) does not further constrain the temperature. From the spectrum without the contribution of PKS 2155–304, we obtain the same upper limit. The reason why these spectra yield nearly the same temperature upper limit is the tightly constrained ratio of $N_{\text{OVII}}/N_{\text{OVI}}$ from the various spectra from $\lesssim 10$ to $\lesssim 35$ (see Tables 1 and 3), compared to 8.9, 26.2, and 63.1 for $\log[T(\text{K})] = 5.6, 5.7,$ and 5.8 , respectively, for gas in CIE (see Sutherland & Dopita 1993 and Fig. 6 in Tripp et al. 2001).

5. DISCUSSION

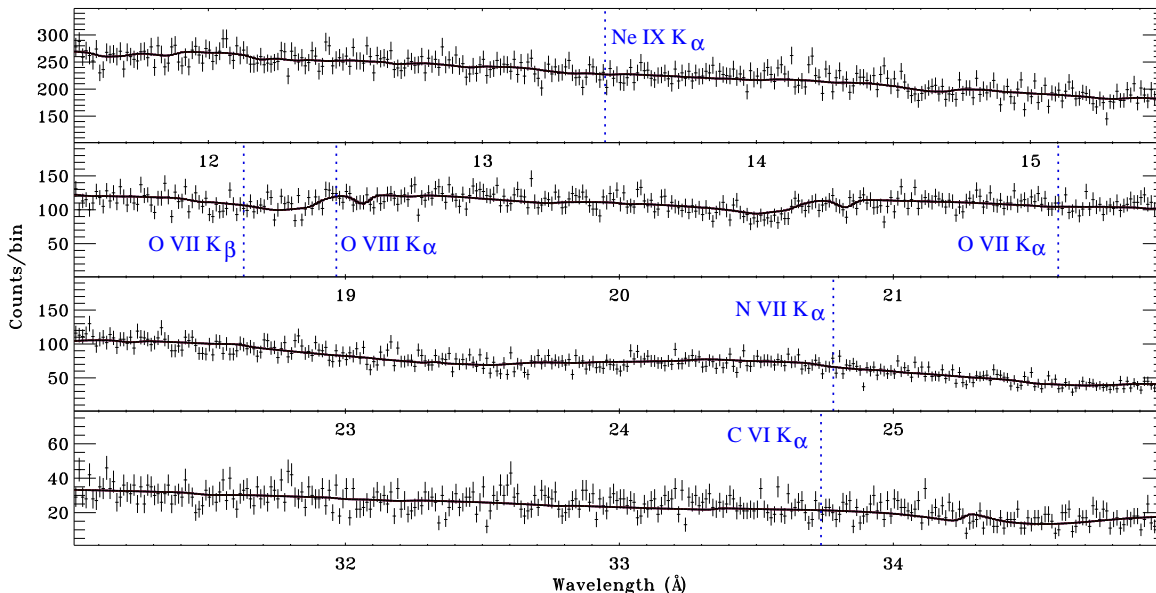


FIG. 6.— Same as Figure 4, except that stacked spectrum contains only spectra corresponding to the strong O VI systems (Table 1).

TABLE 3
THE 95% CONFIDENCE UPPER LIMITS OF $K\alpha$ ABSORPTION LINES

line λ (Å)	Ne IX 13.448	O VIII 18.967	O VII 21.602	N VII 24.781	C VI 33.736
EW (mÅ) ^a	1.0(1.5)	2.2(2.6)	1.1(2.6)	1.2(2.0)	3.6(8.1)
$\log[N(\text{cm}^{-2})]^a$	15.04(15.29)	15.51(15.57)	14.62(15.12)	14.85(15.06)	15.06(15.71)
EW (mÅ) ^b	1.5(3.0)	2.3(3.0)	1.4(2.9)	1.3(3.0)	4.4(8.2)
$\log[N(\text{cm}^{-2})]^b$	15.28(15.71)	15.53(15.62)	14.75(15.15)	14.90(15.21)	15.15 (15.76)
EW (mÅ) ^c	3.8	3.1	3.95	4.3	8.0
$\log[N(\text{cm}^{-2})]^c$	15.75	15.63	15.19	15.33	15.36

NOTE. — Superscripts *a*, *b*, and *c* denote the upper limits obtained from stacked X-ray spectra corresponding to all, complex, and strong O VI absorbers, respectively. Values in parenthesis indicate limits constrained from the spectra without contribution from the PKS 2155-304 sight line.

We have presented a search for X-ray absorption lines produced in the WHIM by using the identified far-UV O VI absorbers as tracers for stacking the archived *Chandra* observations. The three final stacked spectra, corresponding to all, complex, and strong O VI absorbers, have signal-to-noise ratios of ~ 32 , 28, and 10, respectively, per 12.5 mÅ spectral bin around the O VII $K\alpha$ wavelength. There are no detectable X-ray absorption lines at the expected wavelengths in these spectra. We have obtained upper limits to EWs of the $K\alpha$ lines of O VII, O VIII, Ne IX, N VII, and C VI and their column densities. Combining these non-detected lines with the average O VI column density, we have also derived an upper limit to the temperature of the O VI-bearing gas.

The X-ray measurements of the O VI systems with different physical properties in principle can reveal the ionization mechanism of the intervening gas. While most observed O VI absorbers could arise in interfaces between the low- and high-ionization phases (e.g., Danforth & Shull 2008; Tripp et al. 2008), compared to the velocity well-aligned simple O VI absorbers, the dynamically complex O VI systems provide more direct evidence for the multiphase nature of the absorbers (e.g.,

Tripp et al. 2001, 2008; Shull et al. 2003; Sembach et al. 2004; Savage et al. 2005). Cosmological simulations of large-structure formation also predict that the O VI systems with larger equivalent widths are more likely to be collisionally ionized (Cen et al. 2001; Fang & Bryan 2001). If the O VI absorbers utilized in this work are indeed multiphase and trace the shock-heated IGM, the hot O VII-bearing gas is expected to be either surrounding the cool absorbers (traced by the absorption lines of Ly α , C II, Si II, etc.) or itself containing the observed O VI or a combination of both. The column densities of O VII (and/or O VIII) are expected to be at least an order of magnitude more than that of O VI. But the current X-ray observations only constrain the $N_{\text{OVII}}/N_{\text{OVI}} \lesssim 10$ on average (Tables 1 and 3), which does not strongly favor the collisional ionization scenario of the O VI absorbers for shock temperatures $T > 10^{5.7}$ K (Furlanetto et al. 2005). However, these data still cannot rule out the photoionization scenario, in which $N_{\text{OVII}}/N_{\text{OVI}}$ is expected to be $\lesssim 3$ (see Fig. 6 in Tripp et al. 2001 and Furlanetto et al. 2005).

There are several possibilities or their combinations that may cause the non-detections of the X-ray lines:

1. Some of the O VI systems may be photoionized

or partly photoionized. The purely photoionized systems may not contribute to the baryon inventory (§ 1) since they could have already been counted through Ly α absorbers. Since the density of the IGM is very low, photoionization could play an important role in producing the highly ionized oxygen species (especially O VI⁵) in the WHIM besides the gravitational shocks (e.g., Chen et al. 2003; Tripp et al. 2008). In this case, the $N_{\text{OVII}}/N_{\text{OVI}}$ is expected to be lower than that in a solely collisionally ionized gas. Simulations show that, while the EWs of O VI and O VII are fairly well correlated in the putative WHIM in a broad overdensity range ($\delta \sim 10 - 100$), for the O VI-absorbers with $EW(\text{O VI}) > 34 \text{ m\AA}$, there are $\lesssim 20\%$ of the associated O VII-absorbers with $EW(\text{O VII}) > 2 \text{ m\AA}$ (see Figs. 13-15 in Chen et al. 2003 and Table 3).

2. Thermal properties of the WHIM may vary among different systems and sight lines. The O VII and/or O VIII absorptions are expected to be strong in some systems and weak in others, but the “strong” X-ray absorption signals that originate from the shock-heated gas could have been diluted in the stacked spectra.

3. The characteristic temperature of the hot gas may be too high (e.g., $T > 3 \times 10^6 \text{ K}$, as observed in the intragroup and intracluster medium) to produce observable O VII or O VIII. In this case, the interface between hot and cool IGM could still be present to be responsible for the observed O VI absorbers, but the average temperature upper limit ($\log[T(\text{K})] < 5.7$) derived from the ratio of $N_{\text{OVII}}/N_{\text{OVI}}$ (§ 4) only applies to the vicinity of the O VI-bearing gas. This may be the case for the $z = 0.0553$ absorber along the PKS 2155-304 sight line where the O VIII line was detected but the O VII was not (§ 1 and references therein).

4. Lastly, the O VI absorbers might only trace the warm part of the WHIM at temperatures $T \lesssim 3 \times 10^5 \text{ K}$, and the hot ($T \sim 10^6 \text{ K}$) IGM is not necessarily always co-located with the warm gas. If this is the case, because of the small ionization fraction of O VI at high temperatures, the O VI absorption lines produced in the hot gas might not have been detected along most of the sight lines. The possible large dispersion velocity of the hot gas could also make the O VI absorption feature shallower and harder to detect. The high sensitivity of the Cosmic Origins Spectrograph, which is scheduled to be

installed on *HST* in spring 2009, will provide a great opportunity to search for such weak O VI absorbers (at $z > 0.12$) and to examine this possibility.

The results obtained in this work also have important implications regarding future observations of the WHIM with the current and the future X-ray observatories. With the still limited spectral resolution [even in the proposed *International X-ray observatory* (IXO), $E/\Delta E \sim 3,000$, which is still $\sim 10 - 15$ times less than those of current far-UV instruments], it will be challenging to conduct a blind search for the X-ray absorption line “forest” produced in the WHIM. A more effective strategy is still to use the identified O VI and/or Ly α absorbers as references, as implemented in this work (also see Chen et al. 2003; Danforth & Shull 2005, 2008). However, if the six sight lines (Table 1) used in this work fairly sample the WHIM filaments over the whole sky, the gas only contains $\lesssim 10^{15} \text{ cm}^{-2}$ of O VII in column density and the O VII K α EW $\lesssim 2.5 \text{ m\AA}$ in absorption on average (Table 3). To detect a weak line with $EW \sim 2 \text{ m\AA}$ in an AGN spectrum with a flux of $4 \times 10^{-12} \text{ ergs s}^{-1} \text{ cm}^{-2} \text{ keV}^{-1}$ around the line centroid, our 1,000-run simulations for an exposure of 50 Ms with the *Chandra* ACIS-LETG only yield 375 detections at $EW/\Delta EW \gtrsim 3\sigma$ significance level. In comparison, for the IXO with $E/\Delta E \sim 3,000$ and effective area of $\sim 3,000 \text{ cm}^2$, our simulations indicate that a 100 ks observation will have a 90% probability of detecting such a weak line at $\gtrsim 3.5\sigma$ significance level.

We are grateful to Renyue Cen for useful discussion on non-detection of X-ray absorption lines. This work was made possible by *Chandra* archival research grant AR7-8014. Additional support for this research was provided by NASA grant NNX08AC14G, provided to the University of Colorado to support data analysis and scientific discoveries related to the Cosmic Origins Spectrograph on the Hubble Space Telescope, and partly through the Smithsonian Astrophysical Observatory contract SV3-73016 to MIT for support of the Chandra X-Ray Center under contract NAS 08-03060. TMT and LS also acknowledge support for this work from NASA grant NNX08AJ44G.

by the X-ray background.

REFERENCES

- Anders, E., & Grevesse, N. 1989, *Geochim. Cosmochim. Acta*, 53, 197
- Bregman, J. N., & Lloyd-Davies, E. J. 2007, *ApJ*, 669, 990
- Buote, D. A., et al. 2009, *ApJ*, in press (arXiv:0901.3802)
- Cagnoni, I., et al. 2004, *ApJ*, 603, 449
- Canizares, C. R., et al. 2005, *PASP*, 117, 1144
- Cen, R., et al. 2001, *ApJ*, 559, L5
- Cen, R., & Fang, T. 2006, *ApJ*, 650, 573
- Cen, R., & Ostriker, J. 1999, *ApJ*, 514, 1
- Chen, X., et al. 2003, *ApJ*, 594, 42
- Cooksey, K. L., Prochaska, J. X., Chen, H.-W., Mulchaey, J. S., & Weiner, B. J. 2008, *ApJ*, 676, 262
- Danforth, C. W., & Shull, J. M. 2005, *ApJ*, 624, 555
- Danforth, C. W., et al. 2006, *ApJ*, 640, 716
- Danforth, C. W., & Shull, J. M. 2008, *ApJ*, 679, 194
- Davé, R., et al. 2001, *ApJ*, 552, 473
- Durret, F., Kaastra, J. S., Nevalainen, J., Ohashi, T., & Werner, N. 2008, *Space Sci. Rev.*, 134, 51
- Fang, T., & Bryan, G. 2001, *ApJ*, 561, L31
- Fang, T., et al. 2002, *ApJ*, 572, L127
- Fang, T., et al. 2003, *ApJ*, 586, L49
- Fang, T., et al. 2006, *ApJ*, 644, 174
- Fang, T., et al. 2007, *ApJ*, 670, 992
- Finoguenov, A., Briel, U. G., & Henry, J. P. 2003, *A&A*, 410, 777
- Furlanetto, S. R., Phillips, L. A., & Kamionkowski, M. 2005, *MNRAS*, 359, 295
- Fukugita, M., et al. 1998, *ApJ*, 503, 518
- Hellsten, U., Gnedin, N. Y., & Miralda-Escudé, J. 1998, *ApJ*, 509, 56
- Kaastra, J. S., et al. 2002, *A&A*, 386, 427

- Kaastra, J., et al. 2006, ApJ, 652, 189
Lehner, N., et al. 2006, ApJS, 164, 1
Mannucci, F., Bonoli, G., Zappacosta, L., Maiolino, R., & Pedani, M. 2007, A&A, 468, 807
Mathur, S., et al. 2003, ApJ, 582, 82
Matsumoto, C., Leighly, K. M., Marshall, H. L. 2004, ApJ, 603, 456
Narayanan, A., Wakker, B. P., & Savage, B. D. 2008, ApJ, submitted
Nicastro, F., et al. 2002, ApJ, 573, 157
Nicastro, F., et al. 2005a, ApJ, 629, 700
Persic, M., & Salucci, P. 1992, MNRAS, 258P, 14
Prochaska, J. X., Chen, H.-W., Howk, J. C., Weiner, B. J., & Mulchaey, J. 2004, ApJ, 617, 718
Prochaska, J. X., et al. 2006, ApJ, 643, 680
Rasmussen, A. P., et al. 2007, ApJ, 656, 129
Savage, B. D., et al. 1998, ApJ, 115, 436
Savage, B. D., Sembach, K. R., Tripp, T. M., & Richter, P. 2002, ApJ, 564, 631
Savage, B. D., et al. 2005, ApJ, 626, 776
Scott, J. E., et al. 2004, ApJS, 152, 1
Scott, J. E., et al. 2005, ApJ, 634, 193
Sembach, K. R., et al. 2003, ApJS, 146, 165
Sembach, K. R., et al. 2004, ApJS, 155, 351
Shull, J. M., et al. 1998, AJ, 116, 2094
Shull, J. M., et al. 2003, ApJ, 594, L107
Soltau, A. M. 2007, A&A, 475, 837
Stocke, J. T., Penton, S. V., Danforth, C. W., Shull, J. M., Tumlinson, J., & McLin, K. M. 2006, ApJ, 641, 217.
Sutherland, R., & Dopita, M. 1993, ApJS 88, 253
Thom, C., & Chen, H.-W. 2008, ApJS, 683, 22
Tripp, T. M., et al. 2000, ApJ, 534, L1
Tripp, T. M., & Savage, B. D. 2000, ApJ, 542, 42
Tripp, T. M., et al. 2001, ApJ, 563, 724
Tripp, T. M., et al. 2006, ApJ, 643, L77
Tripp, T. M., et al. 2008, ApJS, 177, 39
Tumlinson, J., Shull, J. M., Giroux, M. L., & Stocke, J. T. 2005, ApJ, 620, 95
Wang, Q. D., Connolly, A., & Brunner, R. 1997ApJ, 487, L13
Wang, Q. D., Owen, F., Ledlow, M. 2004, ApJ, 611, 821
Wang, Q. D., et al. 2005, ApJ, 635, 386
Williams, R. J., et al. 2007, ApJ, 665, 247
Yao, Y., & Wang, Q. D. 2005, ApJ, 624, 751
Yao, Y., & Wang, Q. D. 2007, ApJ, 658, 1088
Yao, Y., et al. 2008, ApJ, 672, L21
Yaqoob, T., et al. 2003, ApJ, 582, 105
Yoshikawa, K., & Sasaki, S. 2006, PASJ, 58, 641